Available online at www.sciencedirect.com
SCIENCE DIRECT®
Journal of Sound and Vibration 288 (2005) 791–812
JOURNAL OF SOUND AND VIBRATION
www.elsevier.com/locate/jsvi

Nonlinear normal modes for vibratory systems under harmonic excitation

D. Jiang[a], C. Pierre[b,*], S.W. Shaw[c,1]

[a]*MKP Structural Design Associates, Inc., 3003 Washtenaw Ave, Ann Arbor, MI 48104, USA*
[b]*Department of Mechanical Engineering, University of Michigan, Ann Arbor, MI 48109-2125, USA*
[c]*Department of Mechanical Engineering, Michigan State University, East Lansing, MI 48824-1226, USA*

Received 19 May 2004; received in revised form 3 December 2004; accepted 12 January 2005
Available online 10 March 2005

Abstract

This paper considers the use of numerically constructed invariant manifolds to determine the response of nonlinear vibratory systems that are subjected to harmonic excitation. The approach is an extension of the nonlinear normal mode (NNM) formulation previously developed by the authors for free oscillations, wherein an auxiliary system that models the excitation is used to augment the equations of motion. In this manner, the excitation is simply treated as an additional system state, yielding a system with an extra degree-of-freedom (dof), whose response is known. A reduced-order model for the forced system is then determined by the usual NNM procedure, and an efficient Galerkin-based solution method is used to numerically construct the attendant invariant manifolds. The technique is illustrated by determining the frequency response for a simple 2-dof mass–spring system with cubic nonlinearities, and for a discretized beam model with 12 dof. The results show that this method provides very accurate responses over a range of frequencies near resonances.

*Corresponding author. Tel.: +1 734 936 0401; fax: +1 734 647 3170.
E-mail address: pierre@umich.edu (C. Pierre).
[1]Visiting Professor, University of California-Santa Barbara.

0022-460X/$ - see front matter © 2005 Elsevier Ltd. All rights reserved.
doi:10.1016/j.jsv.2005.01.009

1. Introduction

Many techniques exist for determining the response of nonlinear systems that are subjected to periodic excitation. In addition to brute-force simulations, there are a variety of approximate analytical methods, such as the method of multiple scales, harmonic balance, and averaging. When the system is responding in a periodic manner, it is behaving like a low order system, and the question arises as to whether or not a reduced order model can be found that captures the system response. In fact, the analytical techniques just mentioned do precisely this, by imposing various types of approximations.

For free vibration problems one uses system modes to construct reduced order models, and these techniques have been well developed for both linear and nonlinear systems [1,2]. One such technique, introduced by Shaw and Pierre [3–5], defines the normal mode of a nonlinear oscillatory system in terms of invariant manifolds in the phase space that are tangent to the linear (eigen-)modes at the equilibrium point. In such a formulation, a *master* mode is selected (the mode of interest), and the normal mode is constructed by a formulation in which the remaining linear modes of the system, i.e., the *slave* modes, depend on the master mode in a manner consistent with the system dynamics. This dependence defines the invariant manifold for the nonlinear normal mode (NNM). The construction of the NNM invariant manifold is equivalent to the determination of the constraint relationships for all of the slave coordinates. Once these constraint relationships are obtained, the system dynamics can be restricted to the invariant manifold, resulting in a minimal-sized model that depends only on the master coordinates. By studying the dynamics of the reduced-order model, it is possible to recover the associated modal dynamics of the original nonlinear system. This model reduction approach is similar to the center manifold technique that allows one to study bifurcation problems using reduced-order models of nonlinear systems [6].

Based on the invariant manifold approach, Boivin et al. [7] were able to construct NNMs for weakly nonlinear systems using polynomial expansion functions to approximate the constraint relationships for the slave coordinates. The polynomial expansion has also been used by Nayfeh et al. [8] to construct invariant manifolds for systems with cubic nonlinearities. They found that a complex variable expression for the master coordinates is very convenient for the construction procedure. King and Vakakis [9] used an energy-based approach to compute NNMs for a class of 1D, conservative, continuous systems. They showed that under some circumstances, NNMs cannot be constructed using physical coordinates and that a transformation to linear modal coordinates is necessary in order to define NNMs. Vakakis and co-workers have carried out extensive investigations of NNMs, including the consideration of stability and bifurcations of NNMs [1]. Pesheck et al. [10] used numerical solutions of the invariant manifold equations to extend the invariant manifold approach to more general systems, including those that are strongly nonlinear. In this approach, the master coordinates were expressed in polar coordinate form, and a Galerkin-based solution technique was introduced to solve the invariant manifold equations. This methodology has been applied to a multi-dof rotating beam system [11] over a strongly nonlinear amplitude range in which significant coupling occurs between the linear modes, due to nonlinear effects. The invariant manifold-based approach has also proved effective for systems with non-smooth characteristics [12], and for gyroscopic and generally damped systems [13].

In order to apply the invariant manifold-based model reduction method to nonlinear systems with harmonic excitation, Shaw et al. [14] introduced a new variable to represent the time-varying term, which is governed by a second-order differential equation. With this new variable, the invariant manifold-based approach can be extended to systems subjected to periodic excitation. Similarly, Agnes and Inman [15] treated forcing as an additional dof and applied the multiple scales method to solve for the NNMs of a 2 dof example system. Since the multiple scales method is based on perturbation ideas, their results are valid in the weakly nonlinear amplitude range. In the present study, model reduction of nonlinear systems under harmonic excitation is carried out by the inclusion of one additional dynamic state variable, the phase of the harmonic excitation, as a master coordinate in the invariant manifold. The constraint relationships for the slave coordinates are then defined in the augmented space, and they depend on the usual modal master coordinates, as well as on the phase of the excitation. The resulting "forced" invariant manifold thus features one additional dimension compared to the free vibration manifold, and it can be solved numerically over large amplitude regions using a Galerkin-based numerical solution procedure [10]. This manifold can be viewed as a 2D surface that varies periodically in time with a period equal to that of the excitation. By this means, it is possible to obtain accurate reduced-order models for strongly nonlinear systems subjected to periodic excitation.

The paper is organized as follows. In Section 2, the class of nonlinear systems to be considered is defined, the invariant manifold formulation is reviewed, and the partial differential equations governing the invariant manifold are derived. In Section 3, the Galerkin-based solution methodology is introduced and applied to the forced response of a simple 2-dof system. The methodology is then applied to a more complicated system, a 12-dof beam model, in Section 4, to further demonstrate the power and utility of the technique. Finally, some conclusions are drawn in Section 5.

2. The invariant manifold approach

We consider an N-dof nonlinear vibratory system wherein the nonlinearities depend only on displacements. In this case, a transformation of the equations of motion to linear modal coordinates yields the following standard form:

$$\ddot{\eta}_i + 2\xi_i\omega_i\dot{\eta}_i + \omega_i^2\eta_i = A_i(\eta_j) + f_i\cos\phi_f, \quad i,j = 1,\ldots,n, \tag{1}$$

where η_i is the ith linear modal coordinate and ω_i is the corresponding natural frequency of free vibrations of the associated linearized system. Damping is assumed to be small, and thus linear proportional damping can be employed, represented here by the linear modal damping ratios, ξ_i. The nonlinear forces in system (1) are included in the terms $A_i(\eta_j)$, which couple the linear modes to one another. In order to simplify the construction for the invariant manifold, the nonlinear forces, A_i, have been assumed to be independent of the linear modal velocities, $\dot{\eta}_j$. (This can be relaxed, but the resulting solution procedure is more cumbersome.) The external harmonic excitation has been projected onto the ith linear modal coordinate, and is thus represented by the term $f_i\cos\phi_f$, where f_i is the linear modal force amplitude, and the phase, ϕ_f, has the form: $\phi_f = \omega_f t + \phi_{f0}$, where ω_f is the excitation frequency, and ϕ_{f0} is an initial phase angle. Note that in some applications (e.g., parametric excitation), f_i may depend on the modal coordinates, and

this could be easily incorporated in the present formulation. Also, gyroscopic effects are not included in formulation (1); again, this could be relaxed, but would complicate the solution procedure. Finally, it is assumed that the linear modal frequencies, ω_i, are not commensurable; this is a necessary restriction for the present formulation, since otherwise the nonlinear system response cannot be reduced to a single mode.

In order to obtain the reduced-order model for system (1), an extension of the invariant manifold approach [10,11] is used. Consider the following $(2N+1)$-state augmented system:

$$\begin{aligned} &y_i = \dot{\eta}_i, \\ &\dot{y}_i + 2\xi_i\omega_i y_i + \omega_i^2\eta_i = A_i(\eta_j) + f_i \cos\phi_f, \quad i,j = 1,\ldots,n, \\ &\dot{\phi}_f = \omega_f, \end{aligned} \tag{2}$$

where the state variables y_i are introduced as the modal velocities, and the phase variable ϕ_f is considered as an additional state, corresponding to an oscillatory dof with constant amplitude. By this means, the phase variable, ϕ_f, which represents the dynamics of the excitation, can be included in the expressions for the invariant manifold. As a result, the reduced-order model based on the invariant manifold can capture the dynamic behavior of system (1) with periodic excitation. This approach is analogous to bifurcation analyses using center manifolds, wherein the bifurcation parameter is taken as the augmented variable, using the so-called "suspension trick" [6].

The next step is to divide the N pairs of state variables in system (2), (η_i, y_i), $i \in [1,n]$, into two separate groups, denoted as the *master* coordinates and the *slave* coordinates. The *master* coordinates, (η_k, y_k), $k \in S_M$, are the modal coordinates (in state variable form) that are to be kept in the final reduced-order model, where S_M is the set of indices that includes the master modes. The *slave* coordinates, (η_i, y_i), $i \notin S_M$, are all the remaining modal dof, which are taken to depend on the master coordinates in a manner that satisfies the equations of motion. In this paper, we focus on the case where a single pair of state variables, whose modal frequency ω_k is close to the excitation frequency ω_f, are retained as the master coordinates. These master coordinates are supplemented by the forcing phase, ϕ_f, which also plays the role of a master coordinate. Thus, our investigation is limited to the primary resonance of a nonlinear system under harmonic excitation. Investigating super- or sub-harmonic resonances, or systems with internal resonances, would require the selection of multiple pairs of state variables as the master coordinates [8,16], resulting in invariant manifolds of higher dimensionality.

Before deriving the partial differential equations (PDE) governing the invariant manifold, the master coordinates, (η_k, y_k), are transformed to polar coordinates,

$$\eta_k = a\cos\phi, \quad y_k = -a\omega_k \sin\phi, \tag{3}$$

where a and ϕ are the amplitude and phase of the master coordinates, respectively, and ω_k is the kth linear modal frequency. Substituting Eq. (3) into the differential equations governing $(\eta_k, \dot{\eta}_k)$ in system (2), yields

$$\begin{aligned} &\dot{a} = -2\xi_k a\omega_k \sin^2\phi - (A_k + f_k \cos\phi_f)\sin\phi/\omega_k, \\ &\dot{\phi} = \omega_k - \xi_k\omega_k \sin 2\phi - (A_k + f_k\cos\phi_f)\cos\phi/(a\omega_k), \\ &\dot{\phi}_f = \omega_f. \end{aligned} \tag{4}$$

In Eq. (4), the nonlinear force term, A_k, depends on all the linear modal coordinates, $\eta_j,\ j \in [1,n]$, in system (2). In order to obtain the reduced-order model that governs the dynamics of the master coordinates, a, ϕ, and ϕ_f, in the form of Eq. (4), the slave coordinates are assumed to depend on the master coordinates in the form

$$\eta_i = P_i(a,\phi,\phi_f), \quad \dot{\eta}_i = Q_i(a,\phi,\phi_f), \ \text{ for } i = 1,\ldots,n,\ i \neq k, \tag{5}$$

where the $(n-1)$ pairs of P_i's and Q_i's are the constraint relationships that represent the invariant manifold. The solution procedure for the P_i's and Q_i's follows the usual invariant manifold formulation.

Substituting expression (5) into system (2), yields

$$\begin{aligned}
&\frac{\partial P_i}{\partial a}\,\dot{a} + \frac{\partial P_i}{\partial \phi}\,\dot{\phi} + \frac{\partial P_i}{\partial \phi_f}\,\dot{\phi}_f = Q_i,\\
&\frac{\partial Q_i}{\partial a}\,\dot{a} + \frac{\partial Q_i}{\partial \phi}\,\dot{\phi} + \frac{\partial Q_i}{\partial \phi_f}\,\dot{\phi}_f + 2\xi_i\omega_i Q_i + \omega_i^2 P_i = A_i + f_i\cos\phi_f,\\
&\quad \text{for } i = 1,\ldots,n,\ i \neq k.
\end{aligned} \tag{6}$$

Then, combining Eqs. (4) and (6), the PDEs governing the invariant manifold are obtained. These are given by

$$\begin{aligned}
Q_i = {} & \frac{\partial P_i}{\partial a}[-2\xi_k a\omega_k \sin^2\phi - (A_k + f_k\cos\phi_f)\sin\phi/\omega_k]\\
& + \frac{\partial P_i}{\partial \phi}[\omega_k - \xi_k\omega_k\sin 2\phi - (A_k + f_k\cos\phi_f)\cos\phi/(a\omega_k)] + \frac{\partial P_i}{\partial \phi_f}\omega_f,\\
& - 2\xi_i\omega_i Q_i - \omega_i^2 P_i + A_i + f_i\cos\phi_f\\
= {} & \frac{\partial Q_i}{\partial a}[-2\xi_k a\omega_k \sin^2\phi - (A_k + f_k\cos\phi_f)\sin\phi/\omega_k]\\
& + \frac{\partial Q_i}{\partial \phi}[\omega_k - \xi_k\omega_k\sin 2\phi - (A_k + f_k\cos\phi_f)\cos\phi/(a\omega_k)] + \frac{\partial Q_i}{\partial \phi_f}\omega_f,\\
& \qquad \text{for } i = 1,\ldots,n,\ i \neq k.
\end{aligned} \tag{7}$$

Once Eq. (7) has been solved, the constraint relationships for the slave coordinates, the P_i's and Q_i's, are known and can be substituted into Eqs. (4). The result is the desired reduced-order model, which has dynamic variables a, ϕ, and ϕ_f. The forced dynamics of the full system near the primary resonance are captured by this model, which is a single-dof system with periodic excitation. It is interesting to note that parametric excitation terms are introduced during this process, in that the nonlinear force, A_k, now depends on the phase of the excitation, ϕ_f. Obviously, the governing equations for the invariant manifold, Eqs. (7), are inherently nonlinear, and are not analytically tractable.

Compared with the invariant manifold approach in the free vibration case [10], the additional phase variable, ϕ_f, is included in the present model to account for the harmonic excitation. Consequently, the invariant manifold, defined by Eq. (5), is 3D, or, equivalently, it can be viewed as a 2D surface that is moving in a time-periodic manner. The numerical construction procedure for the invariant manifold is therefore more complicated than that for the free oscillation case,

where the manifold is 2D. However, some useful properties can be utilized to alleviate the computational effort required in the solution process. First, in expression (5), the constraint relationships for the modal velocities, the Q_i's, are the time derivative of the corresponding position constraints, the P_i's. Hence, it is possible to eliminate the Q_i's from the unknowns during the numerical solution procedure, and deduce them from the solution of the P_i's. Another useful property is attributed to the polar form of the master coordinates, defined in Eq. (3). By this means, the 3D space on which the invariant manifold is defined can be divided into a 1D amplitude region, a, and a 2D phase region, (ϕ, ϕ_f). For the 2D phase region, a 2D Fourier series is the natural choice for the expansion functions in the Galerkin-based solution procedure. Therefore, fast Fourier transforms can be applied to efficiently carry out the conversion between the values at the discretized points and the corresponding Fourier coefficients. These simplifications are employed to construct the invariant manifolds for the two example systems.

3. A two-dof mass–spring system

The first example presented is quite simple; it is used simply to demonstrate the steps in the process. The two-dof mass–spring system under consideration is shown in Fig. 1. The equations of motion for the system are

$$\begin{aligned} m_1\ddot{x}_1 + k_1x_1 + \beta_1x_1^3 + k_2(x_1 - x_2) &= f\cos\omega_f t,\\ m_2\ddot{x}_2 + k_2x_2 - k_2x_1 + k_3x_2 + \beta_2x_2^3 &= 0, \end{aligned} \tag{8}$$

where $m_1 = 1.0\,\text{kg}$, $m_2 = 1.5\,\text{kg}$, $k_1 = 2.0\,\text{N/m}$, $k_2 = 3.5\,\text{N/m}$, $k_3 = 5.0\,\text{N/m}$, $\beta_1 = \beta_2 = 1.0\,\text{N/m}^3$, and $f = 1.0\,\text{N}$. The excitation frequency ω_f varies within a certain range near primary resonance, and the invariant manifold is solved for at each frequency over that range.

The physical displacement coordinates, $\{x_1, x_2\}^{\text{T}}$, are first transformed to modal coordinates, $\{\eta_1, \eta_2\}^{\text{T}}$:

$$\begin{Bmatrix} x_1 \\ x_2 \end{Bmatrix} = \begin{bmatrix} 0.7173 & 0.6967 \\ 0.5689 & -0.5857 \end{bmatrix} \begin{Bmatrix} \eta_1 \\ \eta_2 \end{Bmatrix}. \tag{9}$$

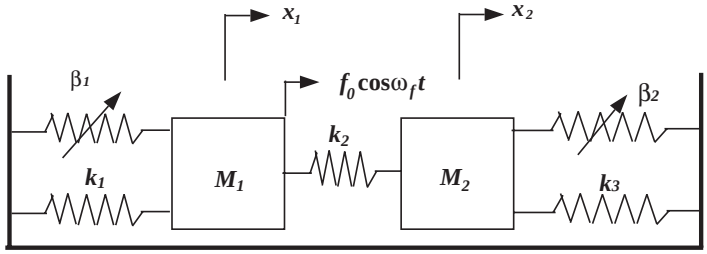

Fig. 1. A 2-dof mass–spring system.

As a result, system (8) is transformed to the standard form

$$\ddot{\eta}_1 + 2\xi_1\omega_1\dot{\eta}_1 + \omega_1^2\eta_1 = A_1 + f_1 \cos\omega_f t,$$
$$\ddot{\eta}_2 + 2\xi_2\omega_2\dot{\eta}_2 + \omega_2^2\eta_2 = A_2 + f_2 \cos\omega_f t, \tag{10}$$

where linear modal damping has been added to the system with damping ratios $\xi_1 = \xi_2 = 0.2$. The two linear modal frequencies are $\omega_1 = 1.6506\,\text{rad/s}$, and $\omega_2 = 2.9056\,\text{rad/s}$. Projecting the external excitation onto the modal coordinates yields $f_1 = 0.1435$ and $f_2 = 0.1393$, and the cubic nonlinear forces, A_1 and A_2, are given by

$$A_1 = -0.7173(0.7173\eta_1 + 0.6962\eta_2)^3 - 0.5689(0.5689\eta_1 - 0.5857\eta_2)^3,$$
$$A_2 = -0.6967(0.7173\eta_1 + 0.6962\eta_2)^3 + 0.5857(0.5689\eta_1 - 0.5857\eta_2)^3. \tag{11}$$

In order to obtain the reduced-order model for system (10), the master coordinate, which is kept in the reduced-order model, must be specified. We first consider the primary resonance near the first linear mode, which occurs when the excitation frequency, ω_f, is close to the first linear modal frequency ω_1. Then, the state variables (η_1, y_1), where y_1 is defined in Eqs. (2), are the natural choice for the master coordinates.

The master coordinates, (η_1, y_1), are transformed to the polar form defined in Eqs. (3):

$$\eta_1 = a\cos\phi, \quad y_1 = \dot{\eta}_1 = -a\omega_1 \sin\phi. \tag{12}$$

The constraint relationships for the slave coordinates, defined in Eqs. (5), are given by

$$\eta_2 = P_2(a, \phi, \phi_f), \quad y_2 = \dot{\eta}_2 = Q_2(a, \phi, \phi_f), \tag{13}$$

and the partial differential equations governing the invariant manifold are as presented in Eq. (7).

A Galerkin-based method is utilized to numerically solve the invariant manifold equations. The 3D space for which the invariant manifold is defined is spanned by one amplitude, $a \in [0, a_{\max}]$, and two phases, $\phi \in [0, 2\pi]$ and $\phi_f \in [0, 2\pi]$. As mentioned above, a 2D Fourier series is the natural choice for the basis functions for the phases, while a variety of functions can be used for the amplitude expansion. It has been shown that the computational cost for the construction of the invariant manifold is significantly reduced if the amplitude domain is discretized into small segments, so that simple piecewise linear functions can be used as the basis functions for each discretized segment in the a direction [10,11]. As a result, in any 3D region,

$$\{(a, \phi, \phi_f) | a \in [a_0, a_1], \phi \in [0, 2\pi], \phi_f \in [0, 2\pi]\}, \tag{14}$$

where a_0 and a_1 are the lower and upper limits of the amplitude segment, respectively, the unknown constraint relationship, P_2, can be expanded as follows:

$$P_2(a, \phi, \phi_f) = \sum_{j=1}^{2} \sum_{l=1}^{N_\phi} \sum_{m=1}^{N_{\phi_f}} C_{jlm} T_j(a) F_l(\phi) F_m(\phi_f), \tag{15}$$

where $T_j(a)$ are piecewise linear functions defined in the amplitude segment, $a \in [a_0, a_1]$, as follows,

$$T_1(a) = \frac{a - a_0}{a_1 - a_0}, \quad T_2(a) = \frac{a_1 - a}{a_1 - a_0}, \tag{16}$$

and $F_l(\phi)$ and $F_m(\phi_f)$ are Fourier terms defined as

$$F_l(\phi) = \begin{cases} \cos\frac{l-1}{2}\phi, & l \text{ is odd}, \\ \sin\frac{l}{2}\phi, & l \text{ is even}, \end{cases} \tag{17}$$

and N_ϕ and N_{ϕ_f} are the number of terms of the Fourier expansions for ϕ and ϕ_f, respectively.

As mentioned in Section 2, the constraint relationship Q_2 can be constructed from P_2. Hence, the invariant manifold in this 3D region is completely determined (in this approximate form) once the unknown coefficients, the C's in expression (15), have been obtained. Note that each small amplitude segment has its own set of C's.

In the Galerkin-based procedure, the expansion for P_2 is substituted into the governing differential equations for the invariant manifold, Eqs. (7). A set of nonlinear algebraic equations governing the unknown coefficients can then be explicitly obtained by requiring that the projection of the residuals of Eqs. (7) onto each basis function, defined in expansion (15), be equal to zero. The C coefficients can then be numerically obtained using an iterative technique. The method selected here is the hybrid Powell's method, which simplifies the solution procedure in a manner such that the explicit form of the set of nonlinear algebraic equations in the C's is not necessary during the iteration process [17].

For a given set of values for the C's, the expression of the velocity constraint, Q_2, can be explicitly determined from the relationship

$$\begin{aligned} Q_2(a, \phi, \phi_f; C) = & \sum_{j=1}^{2} \sum_{l=1}^{N_\phi} \sum_{m=1}^{N_{\phi_f}} C_{jlm} \frac{\mathrm{d}T_j}{\mathrm{d}a}(a) F_l(\phi) F_m(\phi_f) \\ & \times [-2\xi_1 a\omega_1 \sin^2\phi - (A_1(a, \phi, \phi_f; C) + f_1 \cos\phi_f) \sin\phi/\omega_1] \\ & + \sum_{j=1}^{2} \sum_{l=1}^{N_\phi} \sum_{m=1}^{N_{\phi_f}} C_{jlm} T_j(a) \frac{\mathrm{d}F_l}{\mathrm{d}\phi}(\phi) F_m(\phi_f) \\ & \times [\omega_1 - \xi_1\omega_1 \sin 2\phi - (A_1(a, \phi, \phi_f; C) + f_1 \cos\phi_f) \cos\phi/(a\omega_1)] \\ & + \sum_{j=1}^{2} \sum_{l=1}^{N_\phi} \sum_{m=1}^{N_{\phi_f}} C_{jlm} T_j(a) F_l(\phi) \frac{\mathrm{d}F_m}{\mathrm{d}\phi_f}(\phi_f)\omega_f, \end{aligned} \tag{18}$$

which is the algebraic form of one of the differential equations governing the invariant manifold, namely the first equation in system (7). It should be noted that the nonlinear force, A_1, in Eq. (18) is only dependent on the C's, since all the nonlinear forces are independent of velocities in system (8). Otherwise, the relationship for Q_2 would be implicit, in which case the velocity constraint, Q_2, would have to be expanded in the same manner as P_2, given in expression (15), and the unknown coefficients for Q_2 would need to be solved for simultaneously with the C's, in an iterative manner.

Eq. (18) is one of the differential equations governing the invariant manifold. The other partial differential equation is the second equation in system (7), which is given by

$$
\begin{aligned}
&-2\xi_2\omega_2 Q_2(a,\phi,\phi_f;C)-\omega_2^2 P_2(a,\phi,\phi_f;C)+A_2(a,\phi,\phi_f;C)+f_2\cos\phi_f\\
&\quad=\frac{\partial Q_2}{\partial a}(a,\phi,\phi_f;C)\left[-2\xi_1 a\omega_1\sin^2\phi-(A_1(a,\phi,\phi_f;C)+f_1\cos\phi_f)\frac{\sin\phi}{\omega_1}\right]\\
&\qquad+\frac{\partial Q_2}{\partial\phi}(a,\phi,\phi_f;C)\left[\omega_1-\xi_1\omega_1\sin 2\phi-(A_1(a,\phi,\phi_f;C)+f_1\cos\phi_f)\frac{\cos\phi}{a\omega_1}\right]\\
&\qquad+\omega_f\frac{\partial Q_2}{\partial\phi_f}(a,\phi,\phi_f;C).
\end{aligned}
\tag{19}
$$

Once we have a method to determine the derivatives, $\partial Q_2/\partial a$, $\partial Q_2/\partial\phi$, and $\partial Q_2/\partial\phi_f$, Eq. (19) can be evaluated numerically.

The derivative along the a direction, $\partial Q_2/\partial a$, can be accurately determined using a finite difference scheme, since the 3D domain given in Eq. (14) can be taken to be arbitrarily small in the a direction during the discretization. Furthermore, the discrete grid points in a are selected as Gaussian quadrature points for polynomials. Since piecewise linear functions are used as the basis functions for a, the highest possible polynomial order is three in Eq. (18). Thus, a three-point Gaussian quadrature formula is sufficient in the region $a\in[a_0,a_1]$, considering the inner product between the residue of Eq. (19) and the basis functions defined in Eq. (15).

The derivatives along the ϕ and ϕ_f directions, $\partial Q_2/\partial\phi$ and $\partial Q_2/\partial\phi_f$, are determined by means of a 2D fast Fourier transform. At any Gaussian quadrature point $a=a^*$, the expression for Q_2 is expanded as

$$
Q_2(a^*,\phi,\phi_f)=\sum_{m=-N_\phi/2}^{N_\phi/2}\sum_{n=-N_{\phi_f}/2}^{N_{\phi_f}/2}D_{mn}\,\mathrm{e}^{\mathrm{i}m\phi}\,\mathrm{e}^{\mathrm{i}n\phi_f},
\tag{20}
$$

where $i=\sqrt{-1}$, and N_ϕ and N_{ϕ_f} are set to be even. The complex Fourier coefficients, D_{mn}, are efficiently obtained by taking the fast Fourier transform at the grid points for Q_2, which is evaluated using Eq. (18)

$$
Q_2(a^*,\bar\phi^I,\bar\phi_f^J)\quad\text{where}\begin{cases}\bar\phi^I=\dfrac{I\pi}{N_\phi},\\[2ex]\bar\phi_f^J=\dfrac{J\pi}{N_{\phi_f}},\end{cases}
$$

$$
\text{for } I=1\ldots 2N_\phi,\ J=1\ldots 2N_{\phi_f}.
$$

Note that $2N_\phi\times 2N_{\phi_f}$ grid points are used to evaluate the $N_\phi\times N_{\phi_f}$ complex Fourier coefficients in Eq. (20), in order to reduce aliasing errors in the Fourier transform. Once the complex Fourier coefficients, D_{mn}, are obtained, the determinations of the derivatives, $\partial Q_2/\partial\phi$ and $\partial Q_2/\partial\phi_f$, are made trivial by using the inverse Fourier transform, along with the manipulation of the complex Fourier coefficients.

The final step is to project the residue of Eq. (19) onto each basis function defined in expansion (15), shown as

$$\int_{a_0}^{a_1}\int_0^{2\pi}\int_0^{2\pi}[T_j(a)F_l(\phi)F_m(\phi_f)\ \mathrm{Res}(a,\phi,\phi_f;C)]\,\mathrm{d}\phi\,\mathrm{d}\phi_f\,\mathrm{d}a=0,$$
$$\text{for } j=1,2;\ l=1\ldots N_\phi;\ m=1\ldots N_{\phi_f}, \tag{21}$$

where $\mathrm{Res}(a,\phi,\phi_f;C)$ represents the residue of Eq. (19). The solution for the invariant manifold is thus obtained by requiring the $2\times N_\phi\times N_{\phi_f}$ inner products between the residue and the basis functions to be all zero. Numerical integration for the projections can be efficiently carried out, since the numerical values of the residue are evaluated only at Gaussian quadrature points. In practice, we employ the hybrid Powell's method [17], imbedded in the numerical package NAG, to search for the solution from the initial guess.

Once the solution for the C's is obtained, the original system (10) can be reduced to two first-order ordinary differential equations with time periodic coefficients that govern the master coordinates, as described in Eqs. (4). As a result, the periodic responses of the original system can be captured using the reduced-order model.

As a specific example, we set the excitation frequency, $\omega_f=1.93\,\mathrm{rad/s}$, and construct the 3D invariant manifold. The result is depicted in Fig. 2 using four cross-sections corresponding to equally spaced values of the excitation phase angle, ϕ_f. Along the amplitude direction a, the overall construction domain for the invariant manifold is set as $a\in[0,3.0]$, which is evenly divided into 60 segments. For each discretized element (as defined in expression (14) with a_0 and a_1 as the lower and upper bounds of the amplitude segment, respectively), the number of Fourier terms in Eq. (15) are set to $N_\phi=N_{\phi_f}=16$. The initial guess values for the C's for each discretized segment are determined as follows: for the first segment, $a\in[0,0.05]$, the results for the C's obtained from the linearized system are good initial values due to the weak effects of nonlinearities in the small amplitude region. Then, for the subsequent segments, the expansion coefficients obtained from the proceeding segment are used as initial values, since the increments in a are quite small. Once the results for all discretized segments are obtained, the expansion coefficients from contiguous segments are averaged at their interface. As a result, the solution for the invariant manifold is stitched together to cover the entire domain of interest.

Some interesting properties of the invariant manifold can be seen in Fig. 2. First, the invariant manifold varies as the phase angle of the excitation force ϕ_f changes, and therefore as time progresses. The time dependence of the manifold can be easily understood since one additional dimension corresponding to the external excitation, ϕ_f, is included in the definition of the manifold. The manifold can be thought of as a 2D surface that varies periodically in time, and Fig. 2 depicts it at four different instants. Moreover, the manifold is not equal to zero as the amplitude a tends to zero, which is different from what occurs in the free oscillation cases, where the invariant manifold is tangent to the corresponding linear modal space at the static equilibrium position [4].

Time responses at the excitation frequency $\omega_f=1.93\,\mathrm{rad/s}$ can be obtained from the reduced-order model, Eqs. (4). Results for two different sets of initial conditions are shown in Figs. 3 and 4, along with comparisons of the responses obtained from the original system model, Eq. (10). With the reduced-order model governing a and ϕ, the time response for $a(t)$ and $\phi(t)$ can be

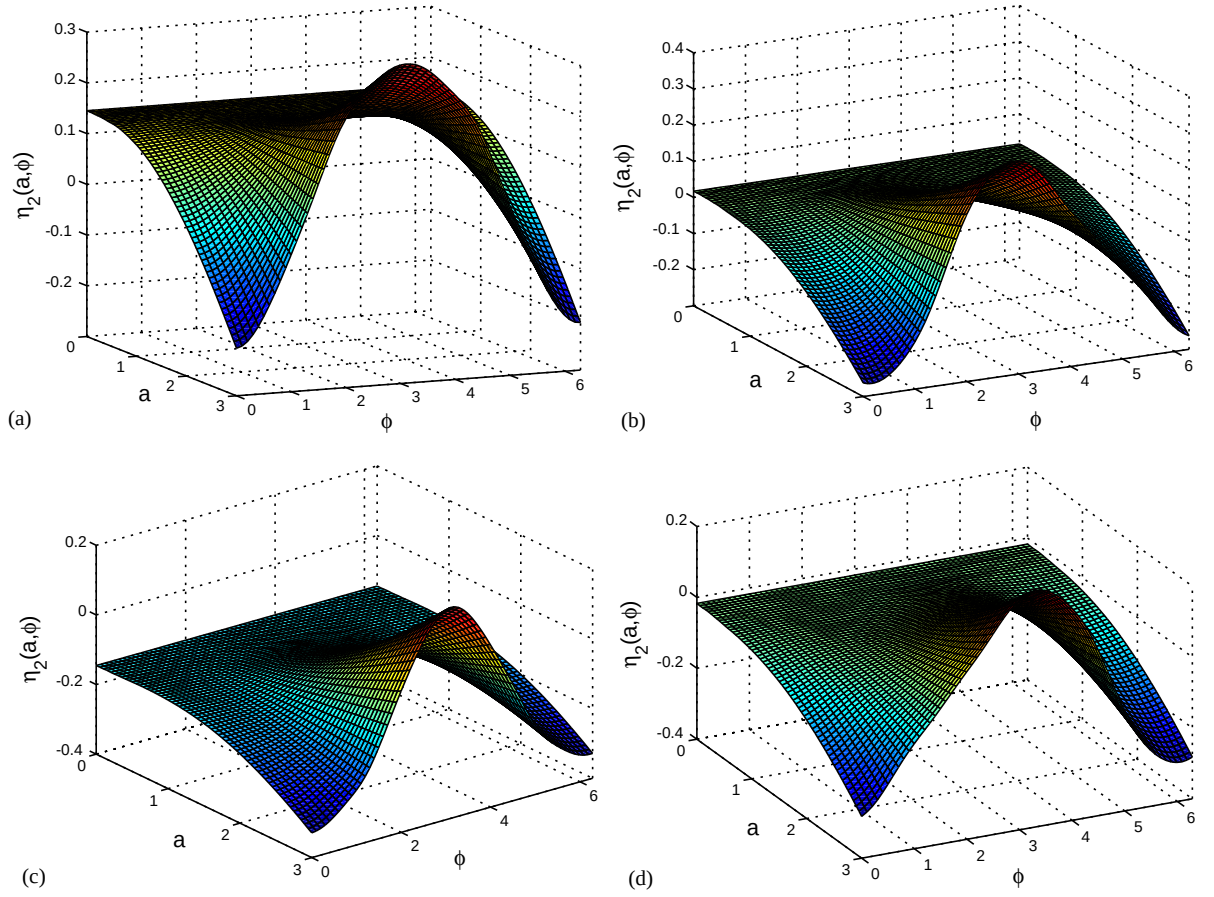

Fig. 2. The first nonlinear mode invariant manifold for the position constraint, $\eta_2 = P_2(a, \phi, \phi_f)$, at various phase angles ϕ_f: (a) $\phi_f = 0.0$, (b) $\phi_f = \pi/2$, (c) $\phi_f = \pi$, (d) $\phi_f = 1.5\pi$.

obtained for any initial conditions $(a(0), \phi(0))$ in the construction domain. The responses of the master and slave coordinates are then reconstructed using the polar transformation definition (3) and the constraint relationships (5), respectively. For time simulations of the original system, initial conditions are taken to be those on which the reduced-order model is initiated, that is, the constraint relations are used to determine the starting conditions for the second mode. As can be seen in Figs. 3 and 4, the forced response obtained from the reduced-order model precisely matches the forced response from the original system model. Note that the responses in Figs. 3 and 4 converge to different steady-state responses, as is typical in such a nonlinear system.

The variation of the steady-state response amplitude of system (10) in terms of frequency is shown in Fig. 5 near the first resonance frequency, ω_1. From the original system model, the frequency response is obtained by sweeping the excitation frequency, ω_f, from 1.5 to 2.2 rad/s. At each excitation frequency, the direct shooting method [18] is used to search for the initial conditions corresponding to the steady-state response. As a result, multiple steady-state solutions

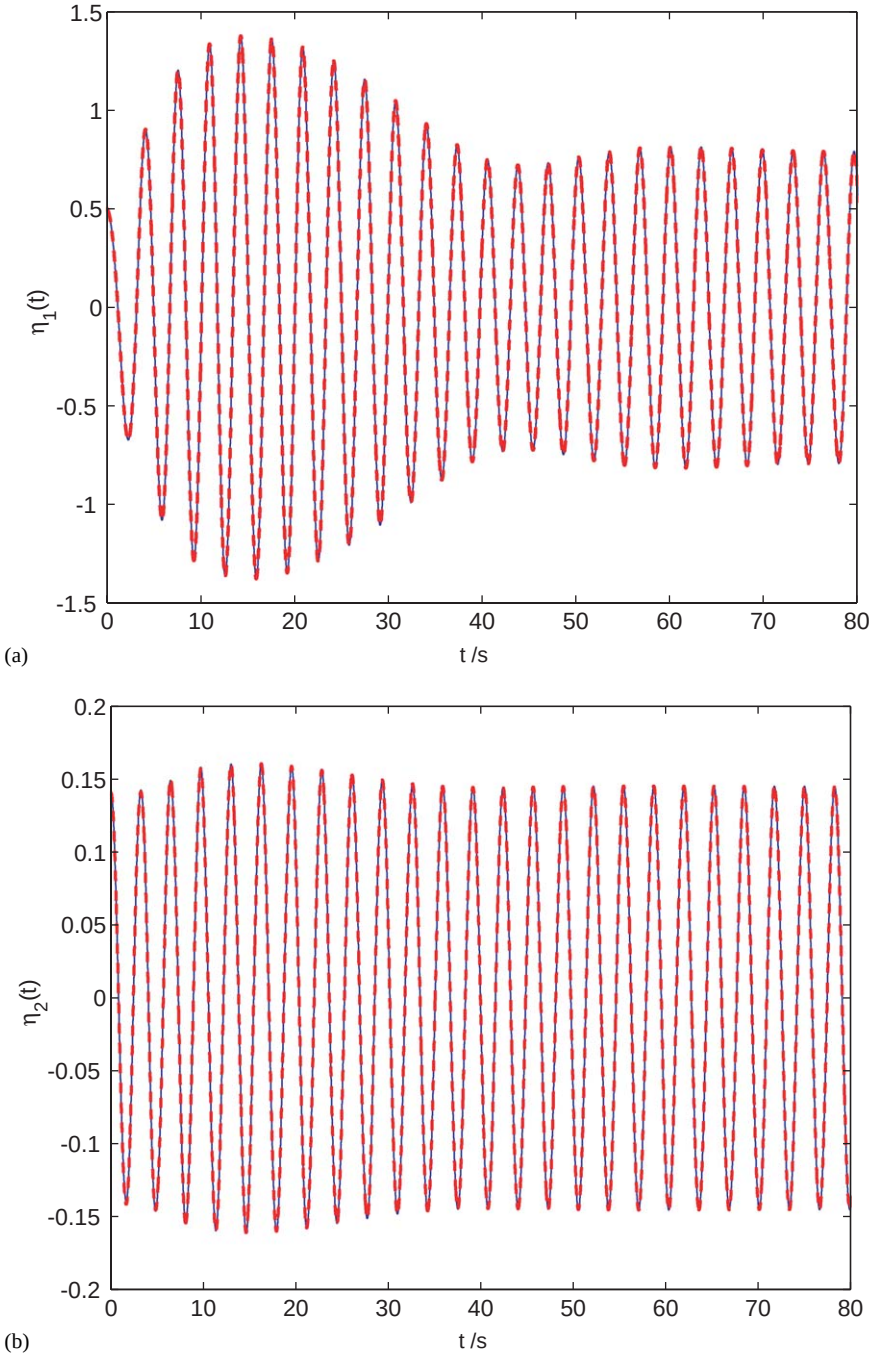

Fig. 3. Comparison of the transient forced response of the modal coordinates, $\eta_1(t)$ and $\eta_2(t)$, with initial conditions $a(0) = 0.5$, $\phi(0) = 0.0$. ——, response obtained from the original system model; - - -, response from the reduced-order model.

are found near the resonance, where one branch of the solutions is unstable. The steady-state responses can also be obtained using simulations of the reduced-order models, constructed at a series of discrete excitation frequencies within the frequency range of interest, $\omega_f \in [1.5, 2.2]$. At

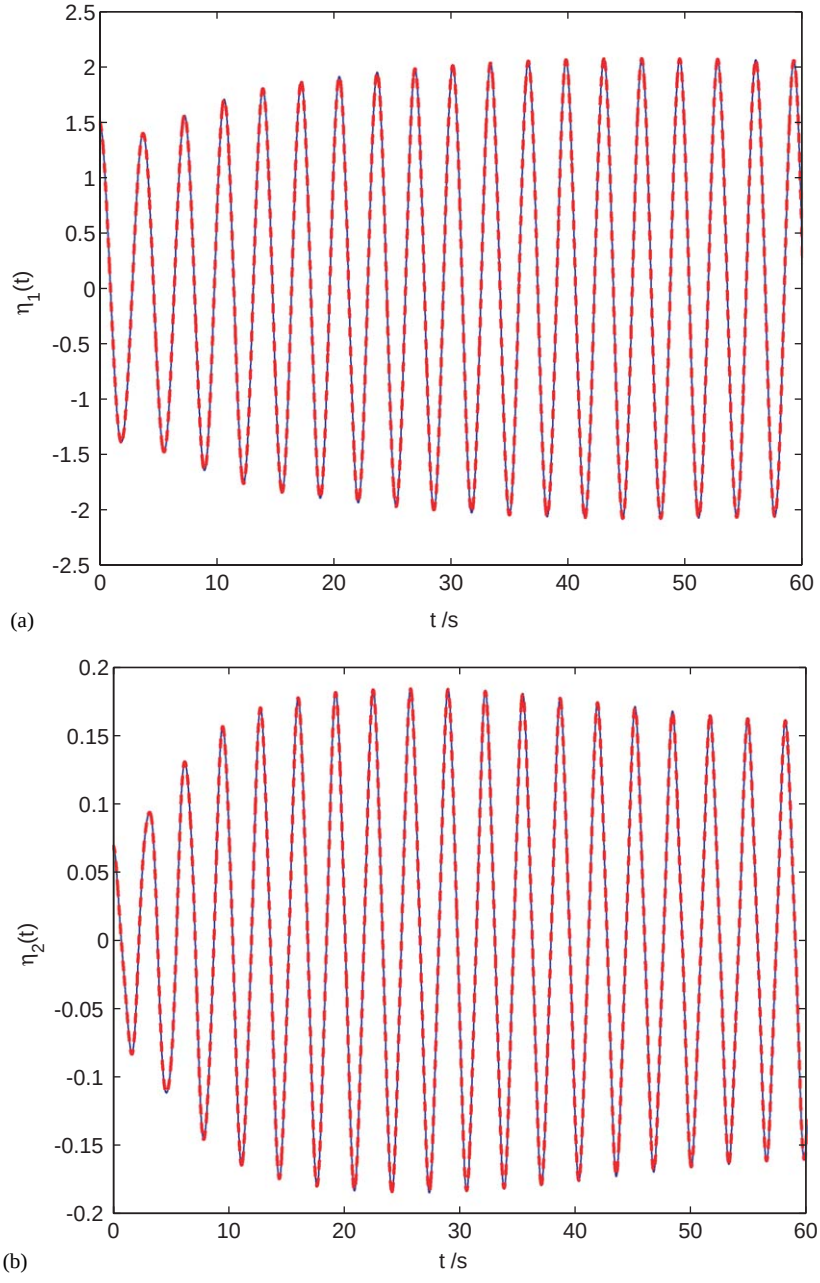

Fig. 4. Comparison of the transient forced response of the modal coordinates, $\eta_1(t)$ and $\eta_2(t)$, with initial conditions $a(0) = 1.5$, $\phi(0) = 0.0$. ——, response obtained from the original system model; - - -, response from the reduced-order model.

each sample frequency ω_f, an invariant manifold-based reduced-order model is constructed following the Galerkin-based procedure described above. As can be seen in Fig. 5, the frequency response obtained from the reduced-order models matches the exact results extremely well, and even the unstable response branch is captured by the reduced-order models. In other words, at any excitation frequency ω_f, the dynamics of the original system are captured by the invariant manifold-based reduced-order model.

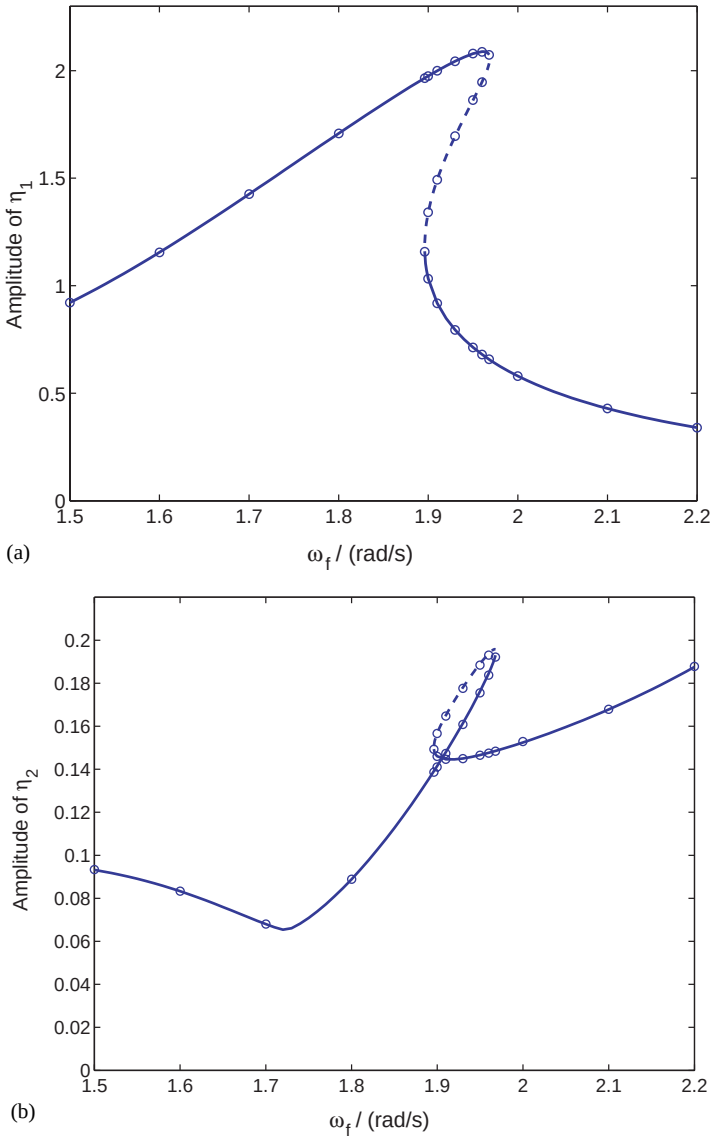

Fig. 5. The amplitude of the steady-state response of the modal coordinates, $\eta_1(t)$ and $\eta_2(t)$, versus the excitation frequency, ω_f. ——, stable steady-state response obtained from the original system model; - - -, unstable steady-state response from the original system model; '○', steady-state response from the reduced-order model.

The steady-state frequency response near the second linear modal frequency, ω_2, is shown in Fig. 6. In this case, the master coordinates are chosen as the second linear modal coordinates in state variable form, $(\eta_2, \dot{\eta}_2)$. The corresponding invariant manifolds are constructed by repeating

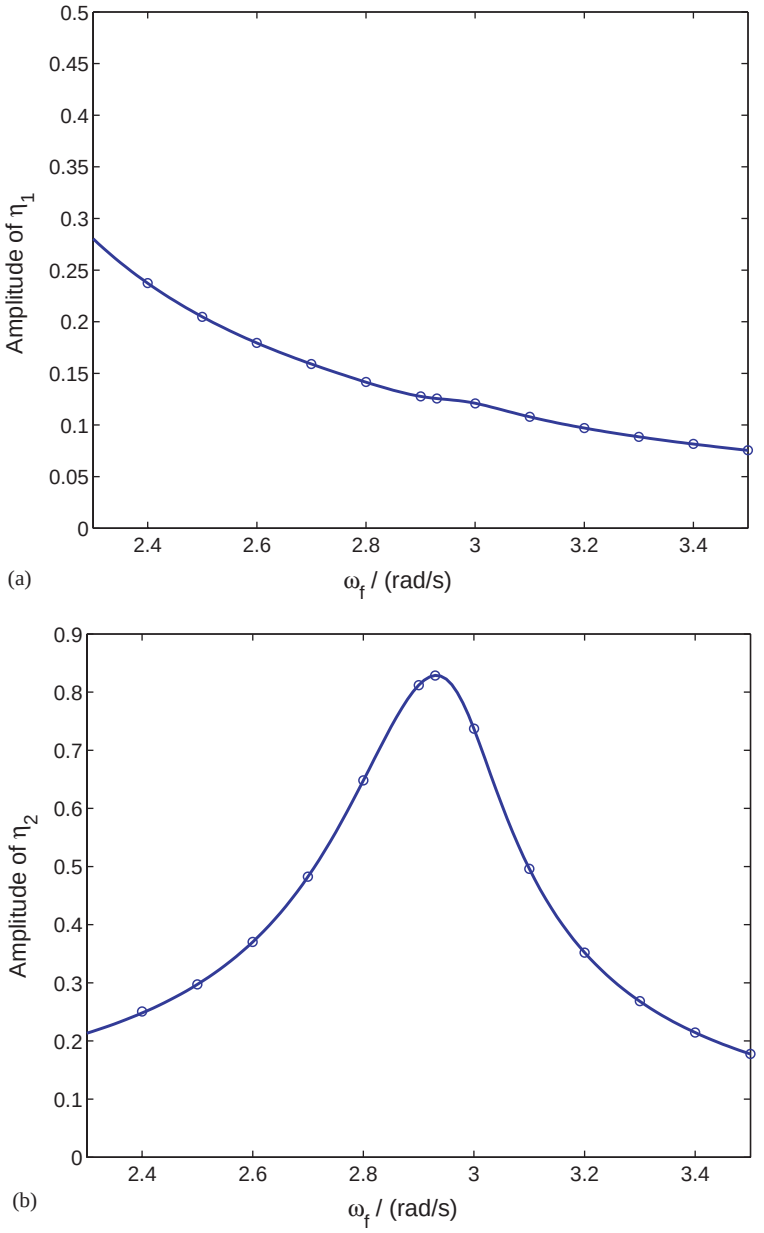

Fig. 6. The amplitude of the steady-state response of the modal coordinate, $\eta_1(t)$ and $\eta_2(t)$, versus the excitation frequency, ω_f. ——, steady-state response obtained from the original system model; '○', steady-state response from the reduced-order model.

the steps described above. Again, excellent agreement is found between the full model and the reduced-order model, as shown in Fig. 6.

We now turn to a more substantial example, where the power and utility of the technique are more fully demonstrated.

4. An Euler–Bernoulli beam with nonlinear spring

The invariant manifold-based model reduction approach, elaborated in Section 3, is applied here to a more complicated example system, an Euler–Bernoulli beam attached to ground at one end by a nonlinear torsional spring. As shown in Fig. 7, the beam has the following geometric and material parameters: length $l = 1\,\mathrm{m}$, cross-sectional area $A = 0.0025\,\mathrm{m}^2$, second moment of area of the cross-section $I = 5.0 \times 10^{-8}\,\mathrm{m}^4$, mass density $\rho = 7860\,\mathrm{kg/m}^3$, Young's modulus $E = 2 \times 10^{11}\,\mathrm{N/m}^2$, and linear spring stiffness $k = 10^8\,\mathrm{N/m}$. The moment from the nonlinear torsional spring at $x = 0$ is given by

$$\gamma_t(t) = 5000\left[\frac{\partial u}{\partial t}(0,t)\right]^2 + 20000\left[\frac{\partial u}{\partial t}(0,t)\right]^3 \mathrm{N},$$

where $u(x,t)$ is the transverse displacement of the beam. The amplitude of the harmonic excitation at $x = l$ is taken to be $f_0 = 3 \times 10^6\,\mathrm{N}$.

The equation of motion governing $u(x,t)$ is given in weak form as

$$\int_{t_1}^{t_2}\left\{\int_0^l(-\rho A\ddot{u}\delta u - EIu_{,xx}\delta u_{,xx})\,\mathrm{d}x - ku(l,t)\delta u(l,t) - \gamma_t\delta u_{,x}(0,t) + F\delta u(l,t)\right\}\mathrm{d}t = 0 \quad \forall t_1 < t < t_2, \tag{22}$$

where $\dot{(\,)}$ denotes the partial derivative with respect to time, and $(\,)_{,x}$ is the partial derivative with respect to x.

In order to obtain the discretized ordinary differential equations for system (22), the Rayleigh–Ritz method is applied, wherein the transverse displacement, $u(x,t)$, is expanded as

$$u(x,t) = \sum_{i=1}^{n-2}\bar{U}_i(x)a_i(t) + \psi_{c0}(x)q_{c0}(t) + \psi_{cl}(x)q_{cl}(t). \tag{23}$$

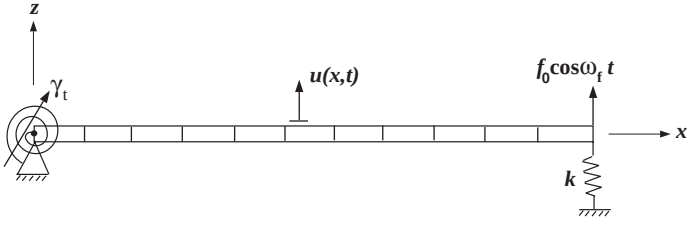

Fig. 7. An Euler–Bernoulli beam with a nonlinear torsional spring, γ_t, at one end.

The basis functions in the above expansion are of two kinds: the fixed-interface normal modes, $\bar{U}_i(x)$ (that is, the modes of free vibration of the beam clamped at $x = 0$ and pinned at $x = l$), and the static constraint modes, $\psi_{c0}(x)$ and $\psi_{cl}(x)$, obtained by imposing a unit slope at $x = 0$ and a unit deflection at $x = l$, respectively, as described below. The selection of these basis functions is motivated by the Craig–Bampton technique, which is commonly used for efficient modal convergence in linear vibration problems. The fixed-interface normal modes, $\bar{U}_i(x)$, are calculated from the following boundary-value problem:

$$-\rho A\bar{\omega}_i^2\bar{U}_i(x) + EI\,\frac{\mathrm{d}^4\bar{U}_i(x)}{\mathrm{d}x^4} = 0, \quad \text{for } i = 1,\ldots,n-2,$$
$$\text{with boundary conditions } \bar{U}_i(0) = 0,\ \frac{\mathrm{d}\bar{U}_i}{\mathrm{d}x}(0) = 0,\ \bar{U}_i(l) = 0,\ \frac{\mathrm{d}^2\bar{U}_i}{\mathrm{d}x^2}(l) = 0, \tag{24}$$

where $\bar{\omega}_i$ is the ith eigenvalue corresponding to the eigenvector $\bar{U}_i$. Note that the rotation at $x = 0$ and transverse displacement at $x = l$ are fixed in Eqs. (24). These dof are captured by the static constraint modes, which are determined by solving the following problems:

$$EI\,\frac{\mathrm{d}^4\psi_{c0}}{\mathrm{d}x^4}(x) = 0,$$
$$\psi_{c0}(0) = 0, \quad \frac{\mathrm{d}\psi_{c0}}{\mathrm{d}x}(0) = 1.0, \quad \psi_{c0}(l) = \frac{\mathrm{d}^2\psi_{c0}}{\mathrm{d}x^2}(l) = 0. \tag{25}$$

and

$$EI\,\frac{\mathrm{d}^4\psi_{cl}}{\mathrm{d}x^4}(x) = 0,$$
$$\psi_{cl}(0) = \frac{\mathrm{d}\psi_{cl}}{\mathrm{d}x}(0) = 0, \quad \psi_{cl}(l) = 1.0, \quad \frac{\mathrm{d}^2\psi_{cl}}{\mathrm{d}x^2}(l) = 0. \tag{26}$$

Expansion (23) is substituted into the weak formulation, Eq. (22), resulting in

$$\int_{t_1}^{t_2}\left\{\int_0^l\left[-\rho A\left(\sum_i \bar{U}_i\ddot{a}_i + \psi_{c0}\ddot{q}_{c0} + \psi_{cl}\ddot{q}_{cl}\right)\left(\sum_j \bar{U}_j\delta a_j + \psi_{c0}\delta q_{c0} + \psi_{cl}\delta q_{cl}\right)\right.\right.$$
$$- EI\left(\sum_i \bar{U}_i'' a_i + \psi_{c0}'' q_{c0} + \psi_{cl}'' q_{cl}\right)\left(\sum_j \bar{U}_j''\delta a_j + \psi_{c0}''\delta q_{c0} + \psi_{cl}''\delta q_{cl}\right)\Bigg]\mathrm{d}x$$
$$\left.- kq_{cl}\delta q_{cl} - \gamma_t(q_{c0})\delta q_{c0} + F\delta q_{cl}\right\}\mathrm{d}t = 0, \quad \forall t_1 < t < t_2, \tag{27}$$

where $()'$ denotes $\mathrm{d}()/\mathrm{d}x$. Eq. (28) can be written in matrix form as

$$\begin{bmatrix}\mathbf{I} & \mathbf{M_{aq}}\\ \mathbf{M_{aq}^T} & \mathbf{M_{qq}}\end{bmatrix}\begin{Bmatrix}\ddot{\mathbf{a}}\\ \ddot{\mathbf{q}}\end{Bmatrix} + \begin{bmatrix}\Lambda & \mathbf{0}\\ \mathbf{0} & \mathbf{K_{qq}}\end{bmatrix}\begin{Bmatrix}\mathbf{a}\\ \mathbf{q}\end{Bmatrix} = \begin{Bmatrix}\mathbf{0}\\ \mathbf{F}\end{Bmatrix}, \tag{28}$$

where $\mathbf{I}$ is the identity matrix, Λ is a diagonal matrix with elements $\lambda_i = \bar{\omega}_i^2$, the vectors $\mathbf{a} = [a_1, a_2, \ldots, a_{n-2}]^{\mathrm{T}}$ and $\mathbf{q} = [q_{c0}, q_{cl}]^{\mathrm{T}}$ contain the amplitudes of the basis functions in the expansion of Eq. (23), and $\mathbf{F} = [-\gamma_t,\ f_0 \cos\omega_f t]^{\mathrm{T}}$ is the forcing vector.

Linear modal analysis can be applied to the linear homogeneous part of Eq. (28), i.e., by setting $\mathbf{F} = 0$, as follows:

$$\left\{-\omega_i^2 \begin{bmatrix} \mathbf{I} & \mathbf{M_{aq}} \\ \mathbf{M_{aq}^{\mathrm{T}}} & \mathbf{M_{qq}} \end{bmatrix} + \begin{bmatrix} \Lambda & \mathbf{0} \\ \mathbf{0} & \mathbf{K_{qq}} \end{bmatrix}\right\} \phi_i = \mathbf{0}. \tag{29}$$

For the ith linear mode, the frequency and mode shape are denoted as ω_i and ϕ_i, respectively. The coordinate transformation to modal coordinates is defined as $\mathbf{X} = \Phi\boldsymbol{\eta}$ where $\mathbf{X} = [\mathbf{a}^{\mathrm{T}}\ \mathbf{q}^{\mathrm{T}}]^{\mathrm{T}}, \Phi$ is the matrix of eigenvectors ϕ_i, and η is the n-dimensional modal coordinate vector. Consequently, system (28) is transformed to the standard form (given in Eq. (1)):

$$\ddot{\eta}_i + 2\xi_i\omega_i\dot{\eta}_i + \omega_i^2\eta_i = A_i(\eta_j) + f_i \cos\omega_f t, \quad i,j = 1, \ldots, n, \tag{30}$$

where proportional damping effects have been added with linear modal damping ratios of $\xi_i = 0.03$.

By changing the number of the fixed-interface normal modes used in expansion (23), the convergence of the response near the first linear modal frequency, $\omega_1 = 222.43\,\mathrm{rad/s}$, is checked for system (30). It is found that a 12-dof model is needed to accurately capture the first primary resonance, including ten fixed-interface modes along with the two static constraint modes.

A single pair of state variables, (η_1, y_1), where $y_1 = \dot{\eta}_1$, in system (30), along with the forcing phase, ϕ_f, are chosen as the master coordinates in the construction procedure for the reduced-order model near the first primary resonance. After employing the polar coordinate transformation for the master mode, $(\eta_1, y_1) \to (a, \phi)$, the remaining slave coordinates are constrained as

$$\eta_i = P_i(a, \phi, \phi_f), \quad y_i = \dot{\eta}_i = Q_i(a, \phi, \phi_f), \ \ i = 2, \ldots, 12,$$

where $\phi_f = \omega_f t$. The governing partial differential equations for the constraint relationships, Eqs. (7), are solved numerically using the Galerkin-based procedures described in Sections 2 and 3. In order to construct the invariant manifold at each excitation frequency near the resonance, the amplitude region $a \in [0, 3.0]$ was evenly divided into 60 segments. For each discretized segment, the number of terms for the Fourier expansions were taken to be $N_\phi = N_{\phi_f} = 8$. From the constructed invariant manifold, the reduced-order model is obtained at each excitation frequency, as shown in Eqs. (4).

The steady-state response of master coordinate η_1 is shown in Fig. 8. As can be seen, both the stable branches and the unstable branch of the response are accurately captured by the simulation based on the reduced-order model. Note that at the excitation frequency $\omega_f = 242\,\mathrm{rad/s}$, the amplitude of η_1 reaches its peak at 1.0, which is physically equivalent to a 0.3 m displacement near the middle point of the 1 m long beam. While at such a

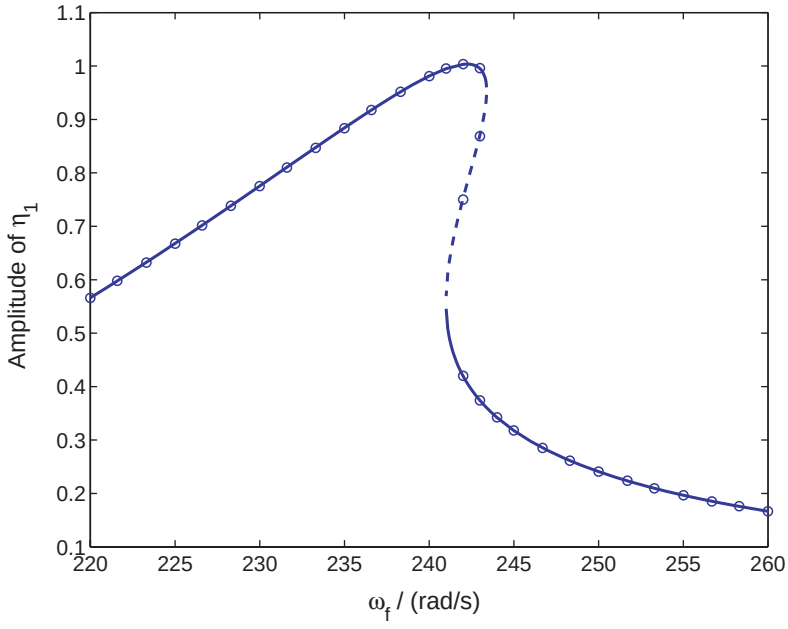

Fig. 8. The amplitude of the steady-state response of the modal coordinates, $\eta_1(t)$, versus the excitation frequency, ω_f. ——, stable steady-state response obtained from the original system model; - - -, unstable steady-state response from the original system model; '○', steady-state response from the reduced-order model.

large amplitude, the assumptions for an Euler–Bernoulli beam are violated, the example clearly demonstrates the capability of accurately capturing the forced response over a strongly nonlinear amplitude range.

The transient response at the excitation frequency, $\omega_f = 242\,\mathrm{rad/s}$, is also shown in Figs. 9 and 10 for two different initial conditions. As can be seen, the response from the reduced-order model matches very closely that from the original system for a range of initial conditions. This demonstrates that the dynamics near the primary resonance can be very accurately captured by the invariant manifold approach. Similar results can be obtained for other resonances, by choosing master modes accordingly.

5. Conclusions

Based on the results obtained from the basic theoretical development, and its application to the mass–spring system studied in Section 3 and the beam system examined in Section 4, the following conclusions are drawn: (1) With the additional phase variable representing the external harmonic excitation, the invariant manifold approach developed for free oscillations can be extended to nonlinear vibration systems subjected to harmonic excitation. (2) Once the invariant manifold is constructed, the corresponding reduced-order model can be obtained to capture the forced dynamics of the original system. (3) The invariant manifold can be constructed numerically using a Galerkin-based technique that employs piecewise linear amplitude functions and Fourier series

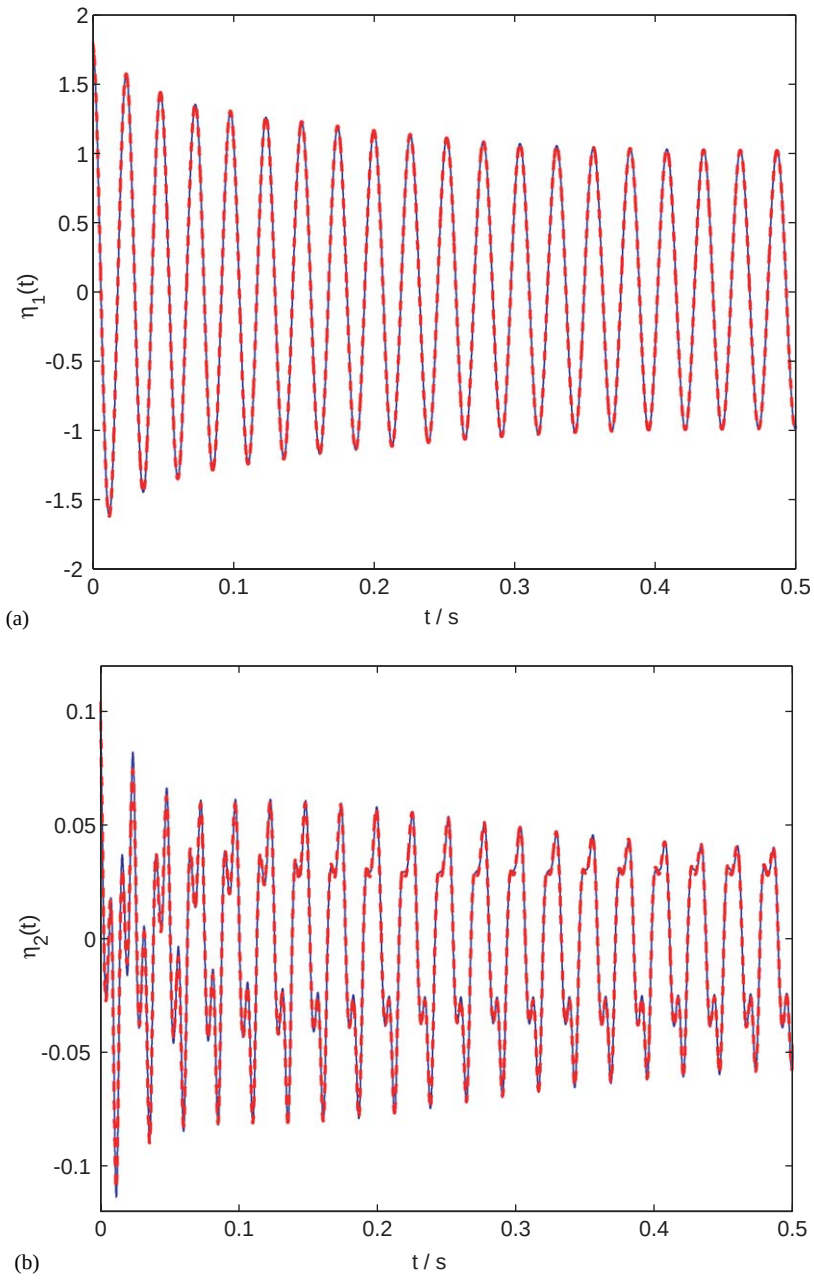

Fig. 9. Comparison of the transient forced response of the modal coordinates, $\eta_1(t)$ and $\eta_2(t)$, with initial conditions $a(0) = 1.79$, $\phi(0) = 0.0$. ——, response obtained from the original system model; - - -, response from the reduced-order model.

for the phase variables. Using fast Fourier transforms, the solution procedure is quite efficient. (4) The domain in which the invariant manifold is defined can be taken out to large amplitudes, and is discretized into small amplitude segments. Consequently, this methodology can be applied to

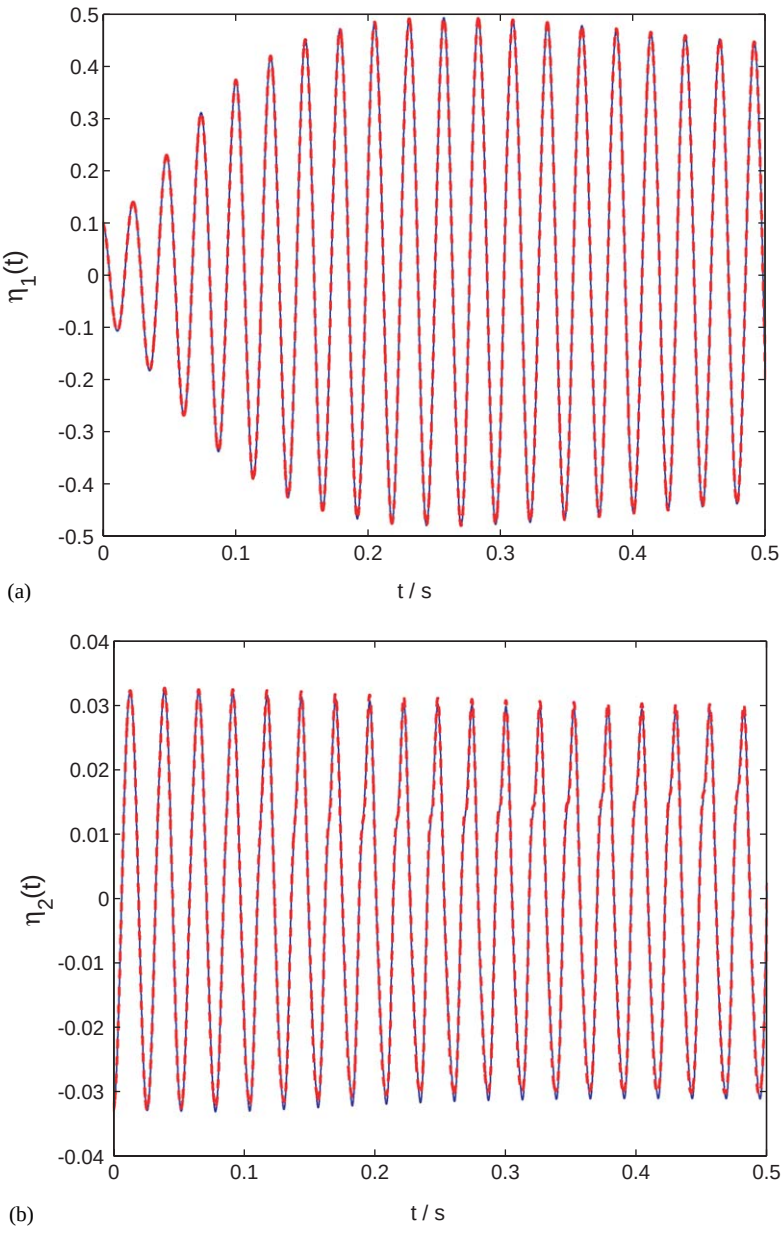

Fig. 10. Comparison of the transient forced response of the modal coordinates, $\eta_1(t)$ and $\eta_2(t)$, with initial conditions $a(0) = 0.1$, $\phi(0) = 0.0$. ——, response obtained from the original system model; - - -, response from the reduced-order model.

systems with complex nonlinearities, such as systems with non-smooth restoring forces, general types of damping, etc. (5) The present method works for any type of harmonic excitation, external and/or parametric. Furthermore, the approach can be extended to include any type of excitation that can be modeled by a finite-state auxiliary dynamic system.

Acknowledgements

This work has been supported by a grant from the Army Research Office, with Dr. Gary Anderson as the grant monitor. The authors would also like to thank Dr. Richard Rand for motivating discussions on this problem. In addition, SWS would like to thank the University of California-Santa Barbara, for their hospitality during a sabbatical leave, during which this paper was completed.

References

[1] A.F. Vakakis, Non-linear normal modes and their applications in vibration theory: an overview, *Mechanical Systems and Signal Processing* 11 (1997) 3–22.
[2] A.F. Vakakis, L.I. Manevitch, Y.V. Mikhlin, V.N. Pilipchuk, A.A. Zevin, *Normal Modes and Localization in Nonlinear Systems*, Wiley, New York, 1996.
[3] S.W. Shaw, C. Pierre, Non-linear normal modes and invariant manifolds, *Journal of Sound and Vibration* 150 (1991) 170–173.
[4] S.W. Shaw, C. Pierre, Normal modes for non-linear vibratory systems, *Journal of Sound and Vibration* 164 (1993) 85–124.
[5] S.W. Shaw, C. Pierre, Normal modes of vibration for non-linear continuous systems, *Journal of Sound and Vibration* 169 (1993) 319–347.
[6] J. Guckenheimer, P. Holmes, *Nonlinear Oscillations, Dynamical Systems, and Bifurcations of Vector Fields*, Springer, New York, 1983.
[7] N. Boivin, C. Pierre, S.W. Shaw, Non-linear normal modes, invariance, and modal dynamics approximations of non-linear systems, *Nonlinear Dynamics* 8 (1995) 315–346.
[8] A.H. Nayfeh, C. Chin, S.A. Nayfeh, On nonlinear normal modes of systems with internal resonance, *Journal of Vibrations and Acoustics* 118 (1996) 340–345.
[9] M.E. King, A.F. Vakakis, An energy-based formulation for computing nonlinear normal modes in undamped continuous systems, *Journal of Vibration and Acoustics* 116 (1994) 332–340.
[10] E. Pesheck, C. Pierre, S.W. Shaw, A new galerkin-based approach for accurate non-linear normal modes through invariant manifolds, *Journal of Sound and Vibration* 249 (2002) 971–993.
[11] P. Apiwattanalunggarn, S.W. Shaw, C. Pierre, D. Jiang, Finite-element-based nonlinear modal reduction of a rotating blade with large-amplitude motion, *Journal of Vibration and Control* 9 (2003) 235–263.
[12] D. Jiang, C. Pierre, S.W. Shaw, Large-amplitude non-linear normal modes of piecewise linear systems, *Journal of Sound and Vibration* 272 (2004) 869–891.
[13] M. Legrand, D. Jiang, C. Pierre, S.W. Shaw, Nonlinear normal modes of a rotating shaft based on the invariant manifold method, *The International Journal of Rotating Machinery* 10 (2004) 1–17.
[14] S.W. Shaw, C. Pierre, E. Pesheck, Modal analysis-based reduced-order models for nonlinear structures—an invariant manifold approach, *The Shock and Vibration Digest* 31 (1999) 3–16.
[15] G.S. Agnes, D.J. Inman, Performance of nonlinear vibration absorbers for multi-degrees-of-freedom systems using nonlinear normal modes, *Nonlinear Dynamics* 25 (2001) 275–292.
[16] D. Jiang, C. Pierre, S.W. Shaw, The construction of nonlinear normal modes for systems with internal resonance, *International Journal of Non-linear Mechanics* 40 (2005) 729–746.
[17] M.J.D. Powell, in: P. Rabinowitz (Ed.), *Numerical Methods for Nonlinear Algebraic Equations*, Gordon and Breach Science Publishers, London, 1970.
[18] P. Sundararajan, S.T. Noah, An algorithm for response and stability of large order non-linear systems—application to rotor systems, *Journal of Sound and Vibration* 214 (1998) 695–723.